Chemical Engineering Journal 112 (2005) 1–11

Chemical Engineering Journal

www.elsevier.com/locate/cej

Kinetic and modelling study of methane steam reforming over sulfide nickel catalyst on a gamma alumina support

D.L. Hoang *, S.H. Chan, O.L. Ding

Fuel Cell Strategic Research Programme, School of Mechanical & Production Engineering, Nanyang Technological University, 50 Nanyang Avenue, Singapore 639798, Singapore

Received 8 March 2005; received in revised form 31 May 2005; accepted 9 June 2005

Abstract

Kinetics and modelling of methane steam reforming over sulfide nickel catalyst on alumina support is studied. Extensive experiments are firstly carried out to study the performance of the steam reforming process and to determine its kinetic data. The results demonstrate that the reforming performance is strongly affected by temperature and ratio of steam to methane. The favourable condition for high hydrogen production, high reforming efficiency and relatively low carbon monoxide concentration is at steam to methane ratio of 3–3.5 and temperature of around 1073 K. Below this temperature value, the methane conversion rate is approximately proportional to the residence time in the studied range. Two-dimensional model of catalytic fixed bed reformer is developed with a system of partial differential equations describing the conservations for mass and energy using kinetic data determined from the current experiment. The modelling results are successfully validated with experimental data.

Keywords: Steam reforming; Kinetics; Modelling; Methane; Hydrogen production

1. Introduction

Hydrogen production has been of great attention in recent years because hydrogen is considered as a clean energy source and its demand in fuel cell application and chemical industry increases [1,2]. The hydrogen production is popularly carried out by hydrocarbon fuel reforming in some ways [3]. Among these, catalytic steam reforming of natural gas, which contains mainly methane, is probably the most important and economic process for the production of hydrogen and synthesis gas in large scale [4]. In industry, steam reforming of natural gas is normally carried out at quite high temperatures ranging from 700 to 900 °C [5] for high product yields. However, there are many factors, including catalyst type, operating conditions and reformer design features, which influence the performance of the reforming process and product distribution [6–11]. Therefore, to optimize the product yields and determine the optimum reformer design for methane steam reforming over a specific commercial catalyst, modelling study may be a fast method to give a good answer. The simulation of the methane steam reforming process requires reliable information on the kinetic data of the catalyst used while the process is quite complex. It not only involves the complicated mass transfer and diffusion between the gas phase and catalyst surface as well as within the catalyst, but also involves several simultaneous reactions taking place in parallel or in series. As a result, the reforming performance is usually different over different catalyst [8,9,11]. For the similar reasons, the reported kinetic data in the literature [12–15] under the catalysts of different types, compositions and of different particle sizes, and over wide ranges of temperature are not uniform. Hence, to receive a reliable prediction of methane steam reforming from modelling work, the kinetic data of the catalyst used should be provided or experimentally determined if not available.

The sulfide nickel catalyst on a gamma alumina support is a new and highly active commercial catalyst, Ni-0309S, which is cheap and popularly used in industrial reformers for hydrocarbon fuel reforming to produce hydrogen and

* Corresponding author. Tel.: +65 67904862; fax: +65 67911859.
E-mail address: mdlhoang@ntu.edu.sg (D.L. Hoang).

1385-8947/$ – see front matter © 2005 Elsevier B.V. All rights reserved.
doi:10.1016/j.cej.2005.06.004

Nomenclature

a_i, b_i	constant (i = 0–3)
b	thickness of the reformer wall (m)
C_i	concentration of gas species i (mol/m^3)
c_{pb}	heat capacity of catalyst bed (J/(kg K))
c_{pg}	heat capacity of gas (J/(kg K))
D_i	gas diffusivity of species i (m^2/s)
D_{dpi}	dispersion coefficient of gas component i
d_i	inner reformer diameter (m)
E_i	activation energy (kJ/kmol)
$F^{in}_{CH_4}$	molar flowrate of inlet CH_4 (mol/s)
G_o	superficial mass flowrate (kg/(s m^2))
g	gravitational acceleration (m/s^2)
h	heat transfer coefficient (W/(m^2 K))
h_{Di}	mass transfer coefficient of gas species i (m/s)
h_i	heat transfer coefficient on the inside of reformer wall (W/(m^2 K))
K	heat conduction coefficient of catalyst bed (W/(m K))
K_{ej}	equilibrium constant of reaction j (j = 2–4)
K_{CH_4}	adsorption constant
K_{oi}, K_{oj}	constant
k_a	thermal conductivity of air in the gap between the heater and the reformer (m)
k_g	heat conduction coefficient of gas (W/(m K))
k_j	rate constant of reaction j
k_{oj}	constant
$\dot{m}$	mass flowrate (kg/s)
p_{CH_4}, ...	partial pressure CH_4, ... (bar)
R	universal gas constant (kJ/(kmol K))
R_j	rate of reaction j (kmol/(kg cat h))
r_i	conversion rates of species i (kmol/(kg cat h))
S_h	heat transfer area per volume of catalyst bed (m^2/m^3)
S_{cat}	catalyst area per volume of catalyst bed (m^2/m^3)
T, T_g, T_h	temperatures of catalyst, bulk gas and outer wall, respectively (K)
u	superficial gas velocity (m/s)
u_z	gas velocity in z direction (m/s)
W_{cat}	catalyst loading (kg)
x_{CH_4}	total conversion of CH_4 (mol/mol)
x_{CO_2}	molar fraction of CH_4 converted to CO_2 (mol/mol)
ΔH_i	adsorption enthalpy of species i (kJ/kmol)
ΔH_j	heat of reaction j (kJ/kmol)

Greek symbols

α	overall heat transfer coefficient through the reformer wall
ε	void fraction of catalyst bed
λ	heat conduction coefficient through the wall
μ_g	dynamic viscosity of gas (kg/ms)
ρ_{cat}	catalyst density (kg/m^3)
ρ_b	catalyst bed density (kg/m^3)
ρ_g	gas density (kg/m^3)
ψ	constant

Subscripts

cat	catalyst
g	gas
i	gas species
j	reaction index (1–3)
r, z	axes cylindrical coordinate
s	solid phase

synthesis gas. Therefore, modelling the methane steam reformer loaded with this catalyst is very useful for optimizing the reformer design and reforming performance.

The objective of this study is to experimentally determine the kinetic data of the sulfide nickel catalyst on a gamma alumina support for methane steam reforming in a range of high reaction temperatures and to simulate the reforming process. The conversion behaviour inside the reformer is then investigated.

Many studies on simulation of methane steam reforming have been carried out in the literature [16–19]. However, these studies applied the kinetic data available for some catalyst as general data in their modelling work for purpose of analyzing the factors influencing the reforming performance. Hence, it is unreliable to use those simulation results in optimizing the design of an industrial reformer using a specific catalyst. In the current work, experimental study, kinetic data determination, and the reformer modelling are carried out together and validated with each other to give reliable results.

2. Experimental study

2.1. Experimental equipment

The schematic layout of the equipment system used for the current experimental study of methane steam reforming is shown in Fig. 1. In this system, gas temperatures and flowrates are fully automatically controlled according to the set values. The reformer is a stainless steel tube with an inner diameter of 10 mm and total length of 400 mm divided into three zones including preheating zone of 100 mm, reaction zone of 150 mm and cooling zone of 150 mm. The preheating zone is filled with inert material (alumina) and heated by a heater, the reaction zone filled with sulfide nickel catalyst and heated by another heater, and the cooling zone filled with inert material. A multipoint thermocouple (a set of four thermocouples) is sliding in a central tube of 2 mm outer diameter to measure and control the preheating and reforming temperatures. The

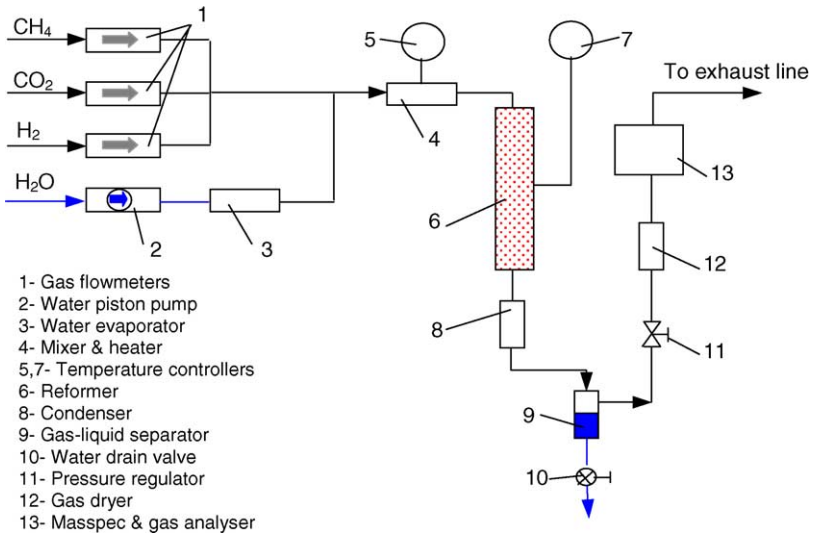

Fig. 1. Schematic of flow system methane steam reforming.

pressure regulator automatically maintains the backpressure in the system at a stable value. The system operation is automatically controlled by the system controller with a computer interface for monitoring and setting operating parameters.

During the steam reforming process, metered water is supplied by the piston pump through the evaporator, mixed with metered methane in the mixer. And then, the mixture of methane and steam is preheated before entering to the reformer containing heated catalyst. The preheating and reforming temperatures are automatically controlled by two temperature controllers. After leaving the reformer, the reformate gas is passed through the condenser, the gas–liquid separator and the gas dryer to remove water content before going to the gas analyzer where its dry composition is determined.

2.2. Catalyst

The catalyst used in this experiment is commercial sulfide nickel catalyst Ni-0309S, supported on gamma alumina supplied by Engelhard Company. This is a new type of commercial catalyst specialized for hydrogen production by hydrocarbon fuel reforming. The reasons for choosing this catalyst in this study is that it is very cheap for use in industries compared with other types of conventional nickel/alpha alumina catalyst and widely used for fuel steam reforming in industrial scale nowadays. Furthermore, the kinetic data of this catalyst are not available while the engineers need one for improving their reactor design.

The catalyst is of spherical type and ready for use as supplied. Its physical property is shown in Table 1.

The amount of catalyst loaded in the reaction zone of the reformer is 8.98 g. Once loaded, the catalyst is heated to 773 K at 3 K/min in nitrogen and maintained at this temperature for 1 h, and then the catalyst is sustained at the same temperature for 2 h in hydrogen. After that, it is heated to 1100 K at 2 K/min and kept at this temperature for a further hour in hydrogen, and then the temperature is reduced to the required operating temperature. Upon reaching this temperature, the pressure is set to 1.5 bars and the water feed is switched on. The reference conditions for steam reforming operation are set and the experiment is started.

2.3. Experimental results

The experimental conditions for methane steam reforming in this study are set in a range ensuring the normal and reliable operation of the equipment system and catalyst. The temperature in the reformer evolves from 773 to 1073 K, ensuring high catalyst activity and avoiding reaching a chemical equilibrium [14]. The reformer pressure is regulated at 1.5 bars; residence time is up to 3.6 kg cat s/mol of inlet CH_4 and the H_2O/CH_4 molar ratio is from 2 to 5. Extensive trial tests was carried out first to check the transient time, reading repeatability and the carbon deposit, and then new catalyst was replaced and prepared for official experiments. The trial tests show that during proposed time duration for experiments the repeatability is good and no carbon deposition is seen on catalysts when they are removed from the reactor and replaced be the new ones. This means that the deactivation of the catalyst is small. Therefore, because the experiments are conducted quite fast, the effect of the catalyst deactivation on the reforming performance can be ignored.

Table 1
Catalyst properties

Nickel content (wt.%)	9.8
S content (wt.%)	4.9
Alumina content (wt.%)	Balance
Surface area (m^2/g)	155
Total pore volume (ml/g)	0.9
Size of the sphere (mm)	1.75
Average crush strength (N)	25

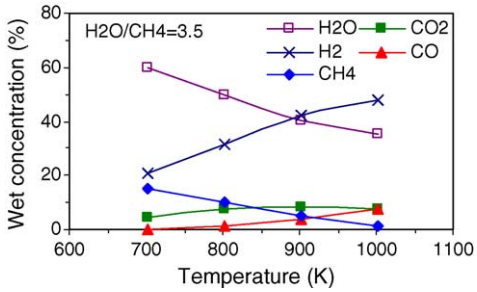

Fig. 2. Wet reformate gas concentration vs. catalyst temperature at residence time of 3.59 kg cat s/mol CH_4.

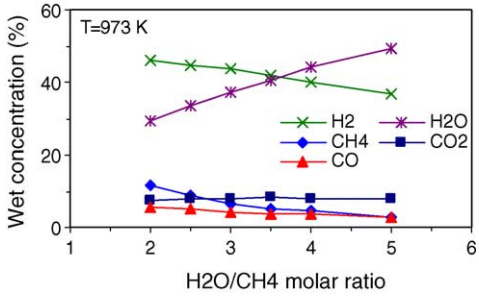

Fig. 3. Wet reformate gas concentration vs. H_2O/CH_4 molar ratio at residence time of 3.59 kg cat s/mol CH_4.

A number of experiment sets have been conducted to determine the reforming performance at different temperatures, H_2O/CH_4 molar ratios and residence time (different CH_4 flowrate at the same catalyst loading). Results of the typical ones are shown in Figs. 2–7 and discussed below.

Fig. 2 depicts the variation of the wet concentrations (with steam present in the gas mixture) of the reformate gas (product) versus reforming temperature under the inlet mixture with H_2O/CH_4 molar ratio of 3.5. It is clear that at higher reforming temperature the CH_4 residual in the reformate gas is lower and the hydrogen concentration is higher. However, increasing reforming temperature leads to an increase in carbon monoxide (CO) concentration that is not desirable for fuel cell application.

Fig. 3 shows the variation of wet reformate gas compositions against H_2O/CH_4 molar ratio at the reforming temperature of 973 K. It can be seen that the CH_4 residual decreases

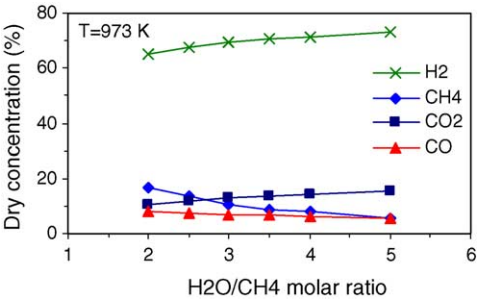

Fig. 4. Dry reformate gas concentration vs. H_2O/CH_4 molar ratio at residence time of 3.59 kg cat s/mol CH_4.

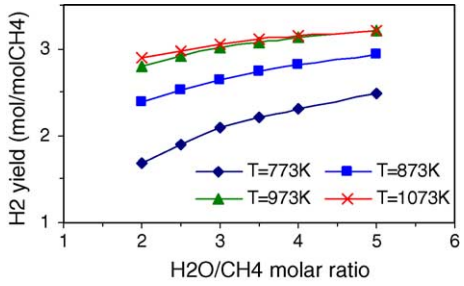

Fig. 5. Hydrogen yield vs. H_2O/CH_4 molar ratio at residence time of 3.59 kg cat s/mol CH_4.

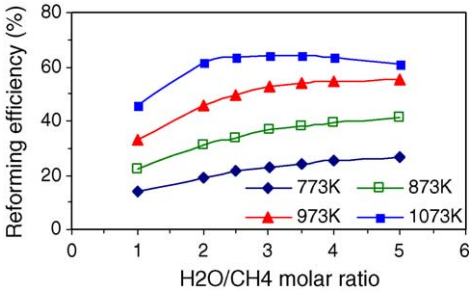

Fig. 6. Reforming efficiency vs. H_2O/CH_4 molar ratio at different temperature and residence time of 3.59 kg cat s/mol CH_4.

with increasing H_2O/CH_4 ratio. This means that the total CH_4 conversion, or in other word, the reaction rate increases with increasing water composition in the inlet mixture. There is also a benefit of decreased CO concentration in this case. However, Fig. 3 also shows that the increase of H_2O/CH_4 ratio in the inlet mixture leads to a significant increase of water content in the product gas because the increase of reaction rate is not directly proportional to the increase of H_2O/CH_4 ratio. Therefore, with increased water content in the wet product gas, the hydrogen concentration in this product decreases as shown in Fig. 3 despite its concentration in the dry product gas (the product gas without water vapour) increases as shown in Fig. 4.

Fig. 4 shows the variation of gas compositions in the dry product. It shows that CH_4 and CO compositions decrease and the formations of H_2 and CO_2 increase with increasing H_2O/CH_4 ratio of the inlet gas. This means that

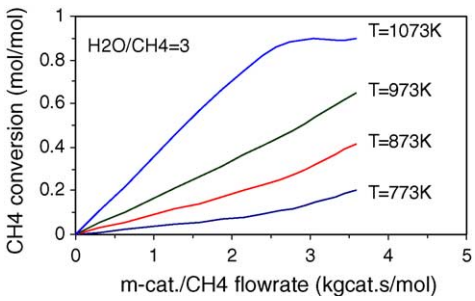

Fig. 7. Total CH_4 conversion vs. residence time at different catalyst temperature and $H_2O/CH_4 = 3$.

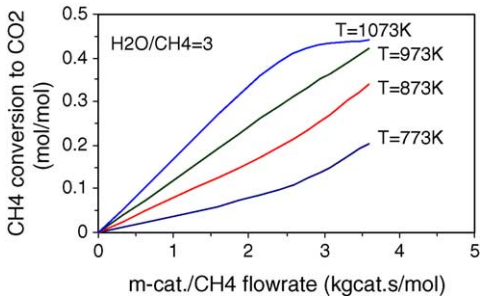

Fig. 8. Mole fraction of CH_4 conversion to CO_2 vs. residence time at different catalyst temperature and $H_2O/CH_4 = 3$.

the conversion of CH_4 and formation of H_2 increase with increasing H_2O/CH_4 ratio. This agrees with Fig. 5 showing that hydrogen yield increases when H_2O/CH_4 increases. The hydrogen yield reaches an approximately stable value close to 3 at temperature above 973 K and steam to methane ratio greater than 3.5.

To evaluate the efficiency of the process, the following coefficient can be used:

$$\eta = \frac{\text{Enthalpy of produced } H_2 \text{ in reformate gas}}{\text{Enthalpy of inlet } CH_4 + \text{enthalpy of } H_2O + \text{heat of evaporation}} \quad (1)$$

The variation of reforming efficiency against H_2O/CH_4 molar ratio at different temperature is presented in Fig. 6. It shows that within the H_2O/CH_4 ratio range of 2–5, the efficiency increases with increasing reforming temperature. However, according to the trend of the curves, it is predicted that at the H_2O/CH_4 ratio greater than 5, the efficiency may decrease when the temperature increase above 1073 K. At high temperature (near 1073 K) the efficiency has a peak at H_2O/CH_4 ratio of around 3.

By analyzing all experimental results, it can be seen that optimum reforming performance in terms of reasonably high efficiency, high hydrogen concentration, high hydrogen yield, low CH_4 residual and relatively low CO concentration can be reached at the temperature of 973–1073 K and H_2O/CH_4 molar ratio of 3–4.

Figs. 7 and 8 show the total CH_4 conversion and CH_4 conversion into CO_2 versus residence time of methane (mass of catalyst per mole of inlet CH_4 flowrate—kg cat s/mol) for steam reforming at water/methane ratio of 3 and different reforming temperatures. It is seen that at a fixed reforming temperature, the total CH_4 conversion and CH_4 conversion to CO_2 increase with increasing residence time. However, the figures also indicate that as residence time increases to greater than 3 kg cat s/mol of inlet CH_4 and temperature around 1073 K or greater, the CH_4 conversion no longer increases and reaches to some stable value. The reason is that the reforming process may reach to equilibrium above this operating condition. Therefore, it can see that for high residence time, the reforming temperature is not necessarily high and is better to be less than 1073 K under the current study condition.

Table 2
Possible reactions in methane steam reforming

No.	Reaction	ΔH_{298} (kJ/mol)
1	$CH_4 + H_2O = CO + 3H_2$	206.1
2	$CO + H_2O = CO_2 + H_2$	−41.15
3	$CH_4 + 2H_2O = CO_2 + 4H_2$	165.0
4	$CH_4 + CO_2 = 2CO + 2H_2$	247.3
5	$CH_4 + 3CO_2 = 4CO + 2H_2O$	330.0
6	$CH_4 = C + 2H_2$	74.82
7	$2CO = C + CO_2$	−173.3
8	$CO + H_2 = C + H_2O$	−131.3
9	$CO_2 + 2H_2 = C + 2H_2O$	−90.13
10	$CH_4 + 2CO = 3C + 2H_2O$	−187.6
11	$CH_4 + CO_2 = 2C + 2H_2O$	−15.3

3. Kinetic model development

The overall reaction in steam reforming process to form C, CO, CO_2 and H_2O may include the equations listed in Table 2 [14,15].

However, according to thermodynamic analysis of the previous studies [14,15], only the first three equations presented in Table 3 occur significantly in steam reforming process while the rates of the other reactions (reactions (4)–(11)) are negligible. Therefore, the steam reforming process can be described on the basis of reactions (1)–(3).

The overall conversion rate of methane and conversion rate of methane to carbon dioxide in the reforming process at different inlet gas conditions can be determined based on experimental data. At first, total methane conversion (x_{CH_4}) and methane conversion to carbon dioxide (x_{CO_2}) versus contact time (residence time) are measured and plotted in graphs (Figs. 7 and 8). Here,

$$x_{CH_4} = \frac{\text{mole of inlet } CH_4 - \text{mole of outlet } CH_4}{\text{mole of inlet } CH_4}$$

and

$$x_{CO_2} = \frac{\text{mole of outlet } CO_2}{\text{mole of inlet } CH_4},$$

where the mole of outlet CH_4 and mole of outlet CO_2 are calculated based on measured CH_4 and CO_2 compositions in the product and the chemical balance of the reforming reaction of one mole of inlet CH_4.

Then, the relationship between total methane conversion and contact time, and between methane conversion to carbon

Table 3
Equilibrium constants

Reaction	Equilibrium constant, K_{ej}
1	$5.75 \times 10^{12} \times e^{-11500/T}$ (bar^2)
2	$1.26 \times 10^{-2} \times e^{4600/T}$
3	$7.24 \times 10^{10} \times e^{-21600/T}$ (bar^2)

dioxide and contact time are analytically expressed in the form of polynomial function as follows:

$$x_{CH_4} = a_0 + a_1\left(\frac{W_{cat}}{F^{in}_{CH_4}}\right) + a_2\left(\frac{W_{cat}}{F^{in}_{CH_4}}\right)^2 + a_3\left(\frac{W_{cat}}{F^{in}_{CH_4}}\right)^3 \quad (2)$$

$$x_{CO_2} = b_0 + b_1\left(\frac{W_{cat}}{F^{in}_{CH_4}}\right) + b_2\left(\frac{W_{cat}}{F^{in}_{CH_4}}\right)^2 + b_3\left(\frac{W_{cat}}{F^{in}_{CH_4}}\right)^3 \quad (3)$$

With the assumption that methane steam reforming reaction occurs only under the presence of catalyst, boundary conditions can be set as: at $W_{cat}/F^{in}_{CH_4} = 0$, $x_{CH_4} = x_{CO_2} = 0$, where x_{CH_4} and x_{CO_2} are mole of total CH_4 conversion per mole of inlet CH_4 and mole of CH_4 conversion to CO_2 per mole of inlet CH_4, respectively, $W_{cat}/F^{in}_{CH_4}$ the residence time (ratio of weight of catalyst, W_{cat}, to inlet mole CH_4 flowrate, $F^{in}_{CH_4}$), and a_i and b_i ($i = 0$–3) are the constants that can be analytically determined by fitting these functions to the experimental data curves shown in Figs. 6 and 7 at different values of contact time and methane conversion.

Finally, once functions (2) and (3) have been determined, the rates of total CH_4 conversion and CH_4 conversion to CO_2 at different inlet gas conditions can be found by differentiating these functions in respect to contact time $W_{cat}/F^{in}_{CH_4}$. Hence, the conversion rates can be calculated at each value of residence time by Eqs. (4) and (5):

$$r_{CH_4} = \frac{dx_{CH_4}}{d(W_{cat}/F^{in}_{CH_4})} = a_1 + 2a_2\left(\frac{W_{cat}}{F^{in}_{CH_4}}\right) + 3a_3\left(\frac{W_{cat}}{F^{in}_{CH_4}}\right)^2 \quad (4)$$

$$r_{CO_2} = \frac{dx_{CO_2}}{d(W_{cat}/F^{in}_{CH_4})} = b_1 + 2b_2\left(\frac{W_{cat}}{F^{in}_{CH_4}}\right) + 3b_3\left(\frac{W_{cat}}{F^{in}_{CH_4}}\right)^2 \quad (5)$$

The determination of reaction rate expressions for methane steam reforming in this study is based on the detailed analyses and studies of possible mechanisms and appropriate rate controlling steps, which have been presented in literature [14,15]. It was widely accepted that both methane and steam were adsorbed on the catalyst with dissociation and the surface reactions producing CO and CO_2 were assumed as the rate controlling steps. Based on information in the literature and following the thermodynamic analysis, it leads to the same appropriate forms of reaction rate expressions as that presented by Xu and Froment [14].

The corresponding rate expressions for reactions (1)–(3) in Table 2 are as follows:

$$R_1 = \frac{k_1}{p^{2.5}_{H_2}}\left(p_{CH_4}p_{H_2O} - \frac{p^3_{H_2}p_{CO}}{K_{e1}}\right) \times \frac{1}{Q_r^2} \quad (6)$$

$$R_2 = \frac{k_2}{p_{H_2}}\left(p_{CO}p_{H_2O} - \frac{p_{H_2}p_{CO_2}}{K_{e2}}\right) \times \frac{1}{Q_r^2} \quad (7)$$

$$R_3 = \frac{k_3}{p^{3.5}_{H_2}}\left(p_{CH_4}p^2_{H_2O} - \frac{p^4_{H_2}p_{CO_2}}{K_{e3}}\right) \times \frac{1}{Q_r^2} \quad (8)$$

$$Q_r = 1 + K_{CO}p_{CO} + K_{H_2}p_{H_2} + K_{CH_4}p_{CH_4} + \frac{K_{H_2O}p_{H_2O}}{p_{H_2}}$$

where R_j (kmol/(kg cat s)) is the rate of reaction j ($j = 1$–3), p_{CH_4}, p_{O_2}, etc. (bar), respectively, the partial pressures of gas species CH_4, O_2, etc., k_j the kinetic rate constant of reactions j and described as $k_j = k_{oj} \times e^{-E_j/RT}$, k_{oj} the constant, E_j (kJ/kmol) the activation energy, R (kJ/(kmol K)) the universal gas constant, T (K) the gas temperature in the reaction zone, K_{ej} the equilibrium constant of reaction j ($j = 1$–3), K_i the adsorption constant of species i ($i = CO$, H_2, CH_4, H_2O) and described as $K_i = K_{oi} \times e^{-\Delta H_i/RT}$, K_{oi} the constant and ΔH_i is the adsorption enthalpy of species i (kJ/kmol). k_j and K_i can be found by fitting the kinetic model to the experimental data.

Reaction rates for the disappearance of CH_4 and formation of CO and CO_2 are obtained from following relations:

$$r_{CH_4} = R_1 + R_3 \quad (9)$$

$$r_{CO} = R_1 - R_2 \quad (10)$$

$$r_{CO_2} = R_2 + R_3 \quad (11)$$

Among these three equations, two are independent, say Eqs. (9) and (11). Substituting these rate equations into Eqs. (4) and (5) for the data treatment at different input and operating conditions can solve for k_j and K_i by iteration, assuming that k_j and K_i are dependent on temperature only. The calculated kinetic rate and adsorption parameters of k_j and K_i, dependent on temperature are depicted in Figs. 9 and 10, respectively, in the temperature range from 773 to 1073 K. Based on these data, the constants, k_{oj}, K_{oi}, activation energy, E_j, and adsorption enthalpy, ΔH_i, can be determined by the following relations:

$$E_j = \frac{\ln(k_{j(1)}/k_{j(2)})}{\frac{1}{T_{(2)}} - \frac{1}{T_{(1)}}} \times R; \qquad k_{oj} = k_{j(1)} \times e^{E_j/RT_{(1)}} \quad (12)$$

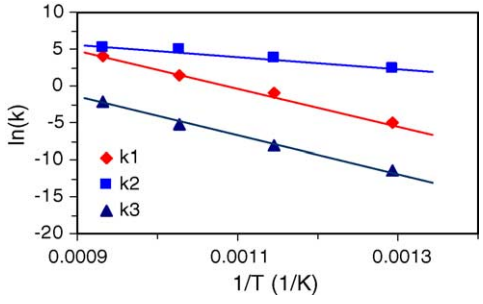

Fig. 9. Temperature dependence of rate constants.

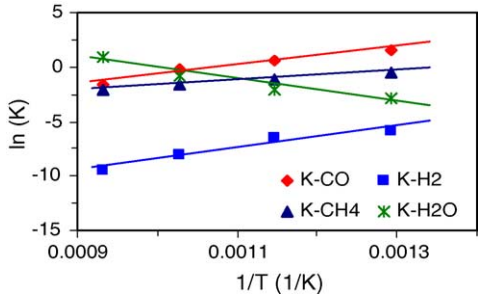

Fig. 10. Temperature dependence of adsorption parameters.

Table 4
Kinetic parameters

Reaction	k_{oj} (mol/kg cat s)	E_j (J/mol)
1	9.048×10^{11} bar$^{0.5}$	209500
2	5.43×10^{5} bar^{-1}	70200
3	2.14×10^{9} bar$^{0.5}$	211500

Table 5
Adsorption constants

Species	K_{oi} (bar^{-1})	ΔH_i (J/mol)
CH_4	1.995×10^{-3}	−36650
CO	8.11×10^{-5}	−70230
H_2	7.05×10^{-9}	−82550
H_2O	1.68×10^{4} bar	85770

$$\Delta H_i = \frac{\ln(K_{i(1)}/K_{i(2)})}{\frac{1}{T_{(2)}} - \frac{1}{T_{(1)}}} \times R;$$
$$K_{oi} = K_{i(1)} \times e^{\Delta H_i/RT_{(1)}} \quad (13)$$

where the subscript indexes (1) and (2) are the two arbitrary reference points (1) and (2) on each curve $\ln(k_j)$ and $\ln(K_i)$ against $1/T$ in Figs. 9 and 10, which can be chosen at $1/T_{(1)} = 1/1073$ and $1/T_{(2)} = 1/773$.

The calculated kinetic rate and adsorption constants in Eqs. (6)–(8) based on the current experimental data are shown in Tables 3–5.

The activation energies of the reforming reactions in the current study are found smaller than the data reported by Xu and Froment [14] for nickel catalyst on alpha alumina support (209,500 and 211,500 kJ/kmol versus 240,100 and 243,900 kJ/kmol). This means that the nickel sulfide/gamma alumina catalyst in the current study is more active than the conventional one. The adsorption enthalpies of the model are also a little smaller than the previously reported data [14].

4. Reformer modelling

In this section, the steam reforming reaction scheme and kinetic rate data determined above are used in modelling of the reformer, aiming to study the gas behaviour in the reformer.

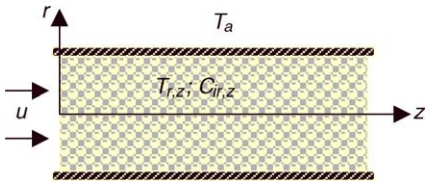

Fig. 11. Thermodynamic system of a 2D reformer.

Fig. 11 shows the thermodynamic system of a 2D reformer model used in this modelling work. The reformer is exactly the same as that used in experiment presented above with 10 mm in inner diameter, 150 mm in length. The reformer is filled with the same sulfide nickel catalyst mentioned in Table 1. It is heated by a high power electrical heater with temperature controller to maintain stable reactor wall temperature. The heat supplied to the reforming process is transferred from the heater through the reformer wall of 1 mm thickness.

Since radiation in reformer catalyst bed can be significant only at the temperature above 1000 °C [20] while the reactor temperature in this study is less than or equal to 800 °C (1073 K), the radiation in this study is insignificant and hence can be omitted. Moreover, because the gas flowrate is relatively low and the void fraction of the bed is high (0.35), the pressure drop is assumed to be negligible. To simplify the model, one may assume that the gas flow in the reformer is uniform and apply 1D model for the reformer. However, the radial dispersion of the gas flow due to catalyst particle size of 1.75 mm and the radial heat transfer due to heat supply through the reformer wall may have some effects on overall reforming performance. To take these effects into account of the modelling work, a 2D reformer model is more appropriate to describe the reforming behaviour under the mentioned conditions [19,21]. Therefore, the 2D model is developed in this study. The phenomena considered in the reformer include chemical reactions on the catalyst surface, heat and mass transfers in the axial and radial directions of the reformer. However, because in the axial direction, the dispersion coefficient is much smaller then the gas velocity, it can be ignored without significant influence on the calculation results. In addition, the heat conductivity of gas is much smaller than that of catalyst bed, it can be omitted. In the gas phase, the change of gas properties and concentrations with time is normally much smaller than that with space, especially when the operation approximately reaches to steady state, hence it can be ignored within a small step time.

4.1. Governing equations

With the assumptions mentioned above, the basic equations of the model based on the mass and energy balance for the gas phase and solid phase of the reformer are as follows:

$$u\frac{\partial C_i}{\partial z} = D_{dpi}\left(\frac{\partial^2 C_i}{\partial r^2} + \frac{1}{r}\frac{\partial C_i}{\partial r}\right) + \rho_{cat} r_i \quad (14)$$

$$\varepsilon\rho_g c_{pg}\frac{\partial T_g}{\partial t} = -u\rho_g c_{pg}\frac{\partial T_g}{\partial z} + S_h h(T - T_g) \quad (15)$$

$$\rho_b c_{pb}\frac{\partial T}{\partial t} = K\left(\frac{\partial^2 T}{\partial r^2} + \frac{1}{r}\frac{\partial T}{\partial r} + \frac{\partial^2 T}{\partial z^2}\right) + S_h h(T_g - T) + \rho_{cat}\sum_{j=1}^{4}(-\Delta H_j)\eta_j R_j \quad (16)$$

where i denotes the gas species; j the reaction index; ρ_g, ρ_{cat}, ρ_b (kg/m^3) the densities of gas, catalyst and bulk catalyst bed, respectively; c_{pg} and c_{pb} (J/(kg K)) the specific heats of gas and of catalyst bed, respectively; ε the void fraction of the catalyst bed; h_{Di} (m/s) the mass transfer coefficient of gas component i; h (W/(m^2 K)) the heat transfer coefficient; T and T_g (K) the temperature of solid phase and gas phase, respectively; C_i (mol/m^3) the concentration of gas species i; r and z (m) the cylindrical coordinates; S_h (m^2/m^3) the heat transfer area per volume of catalyst bed; ΔH_j (J/mol) the heat of reaction j; K (W/(m K)) the heat conduction coefficient of catalyst bed; D_{dpi} the dispersion coefficient of gas component i; u (m/s) is the superficial gas velocity equal to the ratio of volume flowrate to the cross-section area of the reformer.

The dispersion coefficient of gas in a catalyst bed is dependent on molecular gas diffusion, bulk gas velocity and pellet diameter and can be determined based on Wakao et al. [29] as follows:

$$D_{dpi} = \varepsilon\left(\frac{D_i}{\tau_{bed}} + 0.5 d_p u\right)$$

where d_p is the pellet diameter, D_i the gas diffusivity of species i to the mixture of the other gas in the reactor and τ_{bed} is the tortuosity of the bed and correlated to the void fraction of catalyst bed ε as follows [30]:

$$\tau_{bed} = \frac{1}{\sqrt{\varepsilon}}$$

Based on the phenomena of the gas flow and operating conditions of the reformer, the initial and boundary conditions are set as follows:

$$\text{Initial condition, } t = 0: \quad T = T_o; \quad (17)$$

$$\text{At the reformer inlet face, } z = 0: \quad T_g = T_g^{in}; \quad C_i = C_i^{in} \quad (18)$$

$$\text{At the reformer outlet face, } z = L: \quad \frac{\partial C_i}{\partial z} = 0; \quad \frac{\partial T_g}{\partial z} = 0 \quad (19)$$

$$\text{At the reformer centre, } r = 0: \quad \frac{\partial C_i}{\partial r} = 0; \quad \frac{\partial T_g}{\partial r} = 0 \quad (20)$$

With these conditions, Eqs. (14) and (16) can be replaced by Eqs. (14b) and (16b), respectively:

$$u\frac{\partial C_i}{\partial z} = 2D_i\frac{\partial^2 C_i}{\partial r^2} + \rho_{cat} r_i \quad (14b)$$

$$\rho_b c_{pb}\frac{\partial T}{\partial t} = K\left(2\frac{\partial^2 T}{\partial r^2} + \frac{\partial^2 T}{\partial z^2}\right) + S_h h(T_g - T) + \rho_{cat}\sum_{j=1}^{4}(-\Delta H_j)\eta_j R_j \quad (16b)$$

At the interfacial surface of inner reformer wall and catalyst bed $r = R$:

$$\frac{\partial C_i}{\partial r} = 0; \qquad K\frac{\partial T}{\partial r} = \alpha(T - T_h); \quad (21)$$

where T_h is the temperature of reformer wall, α the overall heat transfer coefficient through the reformer wall and K (W/(m K)) are the heat conduction coefficients of the catalyst bed and gas, respectively.

The properties of gas in the reformer, ρ_g and c_{pg}, depend on temperature and composition of the gas mixture. k_g depends on temperature and heat capacity of gas [22] and, hence, also depends on the composition of the gas mixture. Therefore, these properties vary from one location to the other in the reformer and vary with time. They are determined from the properties and mass fractions of the individual species of the gas mixture. The properties of each individual gas can be taken from [22,23] as algebraic functions of temperature. Therefore, at each point in the reformer volume, once the temperature and mole or mass fractions of the gas mixture are known, the overall properties can be determined.

4.2. Heat and mass transfer coefficients

The heat transfer coefficient between catalyst and gas, h (W/(m^2 K)), is determined using Colburn factor J_H [24] as:

$$h = J_H\frac{c_{pg}G_o}{(Pr)^{2/3}} \quad (22)$$

$$J_H = 0.91 Re^{-0.51}\psi \quad (Re < 50)$$
$$J_H = 0.61 Re^{-0.41}\psi \quad (Re > 50) \quad (23)$$

$$Re = \frac{G_o}{S_{geo}\mu_g\psi} \quad (24)$$

where Pr is the Prandtl number of the gas flow in the reformer; ψ the coefficient depending on the particle shape, for spherical particles, ψ has the value of 1 and G_o (kg/(s m$_2$)) is the superficial mass flowrate, which is defined as mass flowrate $\dot{m}$ divided by the cross-section area, S, of the reformer:

$$G_o = \frac{\dot{m}}{S}$$

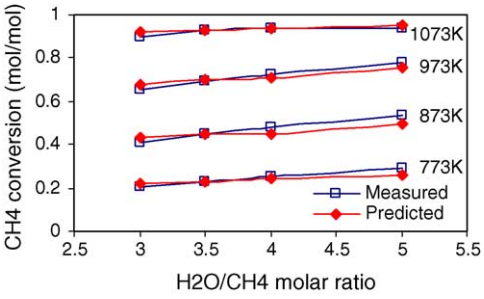

Fig. 12. Comparison of predicted and measured total conversion of CH_4 per mole of fed CH_4 at different reforming temperature, residence time = 3.59 kg cat s/mol of fed CH_4.

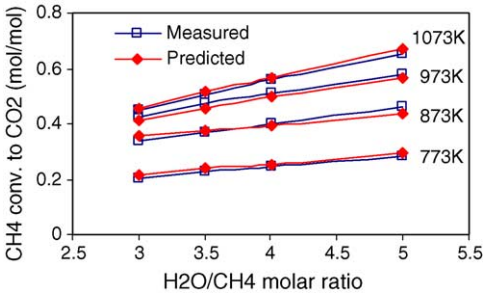

Fig. 13. Comparison of predicted and measured conversion of CH_4 into CO_2 per mole of fed CH_4 at different reforming temperature, residence time = 3.59 kg cat s/mol of fed CH_4.

The overall heat transfer coefficient from the outside surface of the reformer wall, α, is determined by:

$$\frac{1}{\alpha} = \frac{1}{h_i} + \frac{b}{\lambda} \tag{25}$$

where b is thickness of the reformer wall (m), h_i the heat transfer coefficient on the inside of the reformer wall (W/(m^2 K)), while λ is the heat conduction coefficient of the reformer wall (W/(m K)), which can be taken from [25], h_i is given by Cussler [26,27].

$$h_i = \frac{0.027 C_c k_g}{d_i} \left(\frac{d_i u_z \rho_g}{\mu_g} \right)^{0.8} \left(\frac{\mu_g c_{pg}}{k_g} \right)^{0.33} \tag{26}$$

where μ_g (kg/(m s)) is the dynamic viscosity of the gas mixture, u_z (m/s) the gas velocity in z direction and d_i (m) is the inner diameter of the reformer.

The set of three governing Eqs. (14)–(16) with initial and boundary conditions Eqs. (17)–(21), combined with the heat and mass transfer coefficients (Eqs. (22)–(26)) is then solved for the temperature and gas concentration along and across the reformer using a finite difference method [28]. The overall temperature and compositions of the products are derived from the predicted values at different space elements at the rear face of the reformer, based on the principle of mixing gas.

5. Reformer modelling results

The initial temperatures are chosen at the same values as the set points of reforming temperature for quickly reaching to steady conditions. The simulation program is then run with different input data to validate the model and study the conversion behaviour inside the reformer. Some typical modelling results in comparison to the experiment data under different reforming temperatures and different H_2O/CH_4 molar ratios are shown in Figs. 12–16.

The predicted total conversion of methane and conversion of methane into carbon dioxide per mole of fed methane in comparison to the experimental data at different reforming temperatures and H_2O/CH_4 molar ratios are described in Figs. 12 and 13. The results show a very good agreement between the predicted and experimental data.

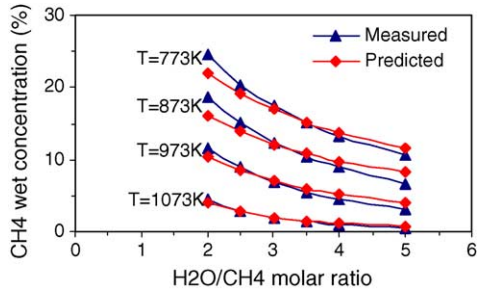

Fig. 14. Comparisons of measured and predicted residual CH_4 wet concentration vs. H_2O/CH_4 molar ratio at residence time of 3.59 kg cat s/mol CH_4.

The variation of three most interested components of reformate gas, including residual CH_4, CO and H_2, is presented in Figs. 14–16. Fig. 14 compares the predicted residual CH_4 and the measured one in wet reformate gas. It is seen that the agreement between them is reasonable, in particular within the practical H_2O/CH_4 ratio range of 3–4. The similar match between the predicted and measured CO is seen in Fig. 15. Figs. 16 shows the comparisons of predicted and measured concentrations for H_2. Generally, the figures presented here show that the modelling results match the corresponding experimental data quite well. Some small discrepancies exist between them are inevitable because of some experimental factors influencing the derived kinetic data. Those may be the errors of measuring instruments, the heterogeneity of

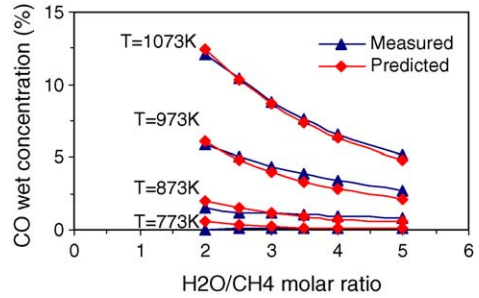

Fig. 15. Comparisons of measured and predicted CO wet concentration vs. H_2O/CH_4 molar ratio at residence time of 3.59 kg cat s/mol CH_4.

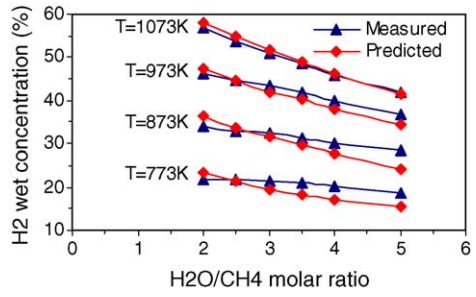

Fig. 16. Comparisons of measured and predicted H_2 wet concentration vs. H_2O/CH_4 molar ratio at residence time of 3.59 kg cat s/mol CH_4.

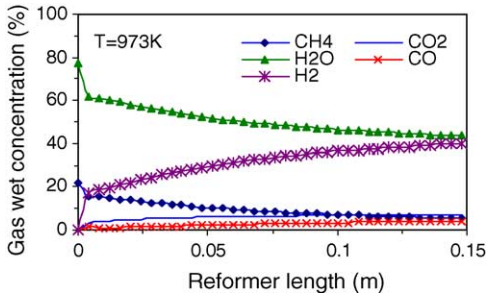

Fig. 17. Average gas concentration along reformer length at $T = 973$ K, $H_2O/CH_4 = 3.5$ and residence time of 3.59 kg cat s/mol CH_4.

temperature in the reformer, and the effects of catalyst aging during experiment. However, with the results discussed here, it can be concluded that the kinetic data derived from the experiments and the results of reformer modelling in this study are reliable. Therefore, the model can be used to analyze the methane steam reforming process and optimize the reformer design in industrial scale using the same catalyst.

The simulation program allows to determine any gas parameters at any space position of the reformer and at any time from the start of reforming operation. Figs. 17 and 18 demonstrate the variation of average gas concentration inside the reformer along its length under the reforming temperatures of 973 and 1073 K, respectively. They show that the gas concentrations continuously change due to chemical reaction when the gas goes through along the reformer. In other words, they show the effect of contact time (residence time) of gas with catalyst on its conversion. From here, the appropriate catalyst loading for a certain gas flowrate can be determined.

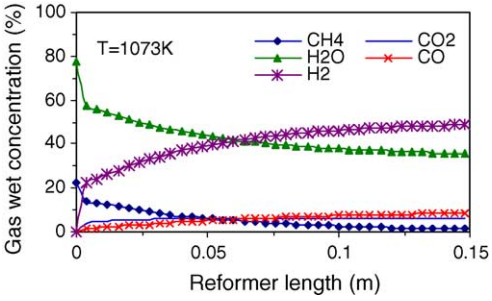

Fig. 18. Average gas concentration along reformer length at $T = 1073$ K, $H_2O/CH_4 = 3.5$ and residence time of 3.59 kg cat s/mol CH_4.

6. Conclusion

An extensive experimental study on steam reforming of methane has been conducted on commercial sulfide nickel catalyst on a gamma alumina support over wide range of reforming temperature and ratio of steam to methane (H_2O/CH_4 molar ratio). The distribution of product is significantly affected by temperature and the ratio of steam to methane. The methane conversion is nearly directly proportional to residence time at temperature lower than 1073 K. The favourite condition found here for catalytic methane steam reforming in terms of high hydrogen production, high efficiency and relatively low carbon monoxide concentration is under the ratio of steam to methane of 3–3.5 and temperature of 973–1073 K.

The kinetic data for commercial sulfide nickel catalyst on a gamma alumina support have been determined based on the current extensive experimental data and the catalytic mechanism presented by Xu and Froment [14]. These kinetic data and model have been used in reformer modelling in this study. The predicted results from the reformer model reasonably agree with the experiment data. It indicates that the kinetic data and the reformer model are reliable and can be used in simulation and comprehensive analysis of an industrial reformer loaded with the same catalyst.

References

[1] M.A. Peña, J.P. Gómez, J.L.G. Fierro, Appl. Catal. A 144 (1996) 7–57.
[2] J.N. Armor, Appl. Catal. A 176 (1999) 159–176.
[3] S. Ahmed, M. Krumpelt, Int. J. Hydrogen Energy 26 (2001) 291–301.
[4] M. Levent, D.J. Gunn, M.A. El-Bousiffi, Int. J. Hydrogen Energy 28 (2003) 945–959.
[5] M.V. Twigg, Catalyst Handbook, Manson Publications, London, 1996 (2nd impression with revisions).
[6] F. Gallucci, L. Paturzo, A. Basile, Int. J. Hydrogen Energy 29 (2004) 611–617.
[7] Y. Matsumura, T. Nakamori, Appl. Catal. A 258 (2004) 107–114.
[8] E. Ramirez-Cabrera, A. Atkinson, D. Chadwick, Appl. Catal. B 47 (2004) 127–131.
[9] H.S. Roh, K.W. Jun, S.E. Park, Appl. Catal. A 251 (2003) 275–283.
[10] H.S. Roh, K.W. Jun, W.S. Dong, J.S. Chang, S.E. Park, Y.I. Joe, J. Mol. Catal. A 181 (2002) 137–142.
[11] W.S. Dong, H.S. Roh, K.W. Jun, S.E. Park, Y.S. Oh, Appl. Catal. A 226 (2004) 63–72.
[12] L.M. Aparicio, J. Catal. 165 (1997) 262–274.
[13] A.C.E. Luna, A.M. Becerra, React. Kinet. Catal. Lett. 61 (2) (1997) 369–374.
[14] J. Xu, G.F. Froment, AIChE J. 35 (1989) 88–96.
[15] M.A. Soliman, M.A. Adris, A.S. Al-Ubaid, S.S.E.H. El-Nashaie, J. Chem. Tech. Biotechnol. 55 (1992) 131–138.

[16] G. Barbieri, F.P. Di Maio, Ind. Eng. Chem. Res. 36 (1997) 2121–2127.
[17] H.M. Kvamsdal, H.F. Svendsen, T. Hertzberg, O. Olsvik, Chem. Eng. Sci. 54 (1999) 2697–2706.
[18] Z. Chen, P. Prasad, Y. Yan, S. Elnashaie, Fuel Process. Technol. 83 (2003) 235–252.
[19] S. Grevskott, T. Rusten, M. Hillestad, E. Edwin, O. Olsvik, Chem. Eng. Sci. 56 (2001) 597–603.
[20] D. Wolf, M. Hohenberger, M. Baerns, Ind. Eng. Chem. Res. 36 (1997) 3345–3353.
[21] D.L. Hoang, S.H. Chan, Appl. Catal. A 268 (2004) 207–216.
[22] M. Kaviany, Principles of Heat Transfer, Wiley & Sons, New York, 2002.
[23] M.J. Moran, H.N. Shapiro, Fundamentals of Engineering Thermodynamics, John Wiley & Sons, New York, 1992.
[24] R.B. Bird, W.E. Stwewart, E.N. Lightfoot, Transport Phenomena, John Wiley & Sons, New York, 1960.
[25] A.J. Chapman, Heat Transfer, Macmillan Publishing Co., New York, 1984.
[26] E.L. Cussler, Diffusion, Mass Transfer in Fluid Systems, Cambridge University Press, Cambridge, NY, 1984.
[27] A.L. Lydersen, Fluid Flow and Heat Transfer, Wiley, New York, 1979.
[28] S.H. Chan, D.L. Hoang, Int. J. Heat Mass Transfer 42 (1999) 4165–4183.
[29] N. Wakao, S. Kaguei, T. Funazkri, Effect of fluid dispersion coefficients on particle-to-fluid heat transfer coefficients in packed beds: correlation of Nusselt numbers, Chem. Eng. Sci. 34 (1979) 325–336.
[30] M. Puncochar, J. Drahos, The tortuosity concept in fixed and fluidized bed, Chem. Eng. Sci. 48 (1993) 2173–2175.